Dynamic stiffness of suction caissons

Ibsen, Lars Bo; Liingaard, Morten; Andersen, Lars Vabbersgaard

Publication date:
2006

Document Version
Publisher's PDF, also known as Version of record

Dynamic stiffness of suction caissons - vertical vibrations

Lars Bo Ibsen
Morten Liingaard
Lars Andersen

ISSN 1901-726X
DCE Technical Report No. 7

AALBORG UNIVERSITY
Department of Civil Engineering

Aalborg University
Department of Civil Engineering
Division of Water and Soil

DCE Technical Report No. 7

Dynamic stiffness of suction caissons - vertical vibrations

by

Lars Bo Ibsen
Morten Liingaard
Lars Andersen

December 2006

Scientific Publications at the Department of Civil Engineering

Technical Reports are published for timely dissemination of research results and scientific work carried out at the Department of Civil Engineering (DCE) at Aalborg University. This medium allows publication of more detailed explanations and results than typically allowed in scientific journals.

Technical Memoranda are produced to enable the preliminary dissemination of scientific work by the personnel of the DCE where such release is deemed to be appropriate. Documents of this kind may be incomplete or temporary versions of papers—or part of continuing work. This should be kept in mind when references are given to publications of this kind.

Contract Reports are produced to report scientific work carried out under contract. Publications of this kind contain confidential matter and are reserved for the sponsors and the DCE. Therefore, Contract Reports are generally not available for public circulation.

Lecture Notes contain material produced by the lecturers at the DCE for educational purposes. This may be scientific notes, lecture books, example problems or manuals for laboratory work, or computer programs developed at the DCE.

Theses are monograms or collections of papers published to report the scientific work carried out at the DCE to obtain a degree as either PhD or Doctor of Technology. The thesis is publicly available after the defence of the degree.

Latest News is published to enable rapid communication of information about scientific work carried out at the DCE. This includes the status of research projects, developments in the laboratories, information about collaborative work and recent research results.

Published 2006 by
Aalborg University
Department of Civil Engineering
Sohngaardsholmsvej 57,
DK-9000 Aalborg, Denmark

Printed in Denmark at Aalborg University

ISSN 1901-726X
DCE Technical Report No. 7

Preface

The technical report "Dynamic stiffness of suction caissons—vertical vibrations" is divided into eight numbered sections, and a list of references is situated after the last section. One appendix is placed at the end of the report. Tables, equations and figures are indicated with consecutive numbers. Cited references are marked as e.g. Senders (2005), with author specification and year of publication in the text.

The work within this report has only been possible with the financial support from the Energy Research Programme (ERP)[1] administered by the Danish Energy Authority. The project is associated with the ERP programme "Soil–Structure interaction of Foundations for Offshore Wind Turbines". The funding is sincerely acknowledged.

Aalborg, December 13, 2006 Lars Bo Ibsen, Morten Liingaard & Lars Andersen

[1] In danish: "Energiforskningsprogrammet (EFP)"

Contents

List of Figures

List of Tables

Chapter 1
Dynamic stiffness of suction caissons—vertical vibrations

The dynamic response of offshore wind turbines are affected by the properties of the foundation and the subsoil. The purpose of this report is to evaluate the dynamic soil–structure interaction of suction caissons for offshore wind turbines. The investigation is limited to a determination of the vertical dynamic stiffness of suction caissons. The soil surrounding the foundation is homogenous with linear viscoelastic properties. The dynamic stiffness of the suction caisson is expressed by dimensionless frequency-dependent dynamic stiffness coefficients corresponding to the vertical degree of freedom. The dynamic stiffness coefficients for the foundations are evaluated by means of a dynamic three-dimensional coupled Boundary Element/Finite Element model. Comparisons are made with known analytical and numerical solutions in order to evaluate the static and dynamic behaviour of the Boundary Element/Finite Element model. The vertical frequency dependent stiffness has been determined for different combinations of the skirt length, Poisson's ratio and the ratio between soil stiffness and skirt stiffness. Finally the dynamic behaviour at high frequencies is investigated.

1.1 Introduction

Wind turbines have increased tremendously in both size and performance during the last 25 years. The general output of the wind turbines is improved by larger rotors and more powerful generators. In order to reduce the costs, the overall weight of the wind turbine components is minimized, which means that the wind turbine structures become more flexible and thus more sensitive to dynamic excitation at low frequencies. The foundation principles for the recent major offshore wind farm projects in Europe have been dominated by two types of foundation solutions: the gravitational foundation and the monopile. Recent research and development projects Houlsby, Ibsen, and Byrne (2005) have shown that suction caissons (see Figure 1.1) may be used as offshore wind turbine foundations in suitable soil conditions and water depths up to approximately 40 meters. Suction caissons (also denoted as bucket foundations or skirted foundations) have previously been used as anchors and foundations for several offshore platforms. Here, the suction caissons are mainly subject to vertical and horizontal loads. On the other hand, when suction caissons are applied as monopod foundations for wind turbines, they must be able to sustain a significant overturning moment. At greater water depths the monopod solution may become uneconomical and a foundation concept with three

or four smaller suction caissons may become appropriate. The overturning moment is then stabilized by the opposing vertical reactions of the suction caissons, see (Houlsby et al. 2005; Senders 2005). The suction caisson is installed by using suction as the driving force and does not require heavy installation equipment. Lowering the pressure in the cavity between the foundation and the soil surface causes a water flow to be generated, which again causes the effective stresses to be reduced around the tip of the skirt. Hence, the penetration resistance is reduced. A fully operational 3.0 MW offshore wind turbine was installed on a prototype of the suction caisson foundation at the test field in Frederikshavn, Denmark in late 2002. The project is described in details in Ibsen et al. (2005).

The purpose of this report is to evaluate the vertical impedance of suction caisson foundations for offshore wind turbines, with the intention that the dynamic properties of the foundation can be properly included in a composite structure–foundation system. The frequency dependent dynamic stiffness is evaluated by means of a dynamic three-dimensional coupled Boundary Element/Finite Element (BE/FE) program BEASTS by Andersen and Jones (2001a). Initially, the solution methods for analysing soil–structure interaction are briefly introduced in Section 1.2. Afterwards, the method applied in this report, i.e. the coupled BE/FE model, is described in Section 1.3. The definitions of static and dynamic stiffness for the suction caisson are presented in Section 1.4. Prior to the analysis, two benchmark tests are shown in Section 1.5. The results obtained by analysing the vertical dynamic stiffness of suction caissons are presented in Section 6 and the findings are discussed in Section 1.7. The main conclusions of the report are given in Section 1.8. In this report the impedance is equal to the dynamic stiffness of the foundation, i.e. the impedance contains both a real and an imaginary part.

1.2 Analysis methods for dynamic soil-structure interaction

The classical methods for analysing vibrations of foundations are based on analytical solutions for massless circular foundations resting on an elastic half-space. The classical solutions by Reissner, Quinlan and Sung were obtained by integration of Lamb's solution for a vibrating point load on a half-space (Richart et al. 1970; Das 1993). The mixed boundary value problems with prescribed conditions under the foundation and zero traction at the remaining free surface were investigated by Veletsos and Wei (1971) and Luco and Westmann (1971). The integral equations of the mixed boundary value problems were evaluated and tabulated for a number of excitation frequencies. A closed-form solution has been presented by Krenk and Schmidt (1981). Whereas analytical and semi-analytical solutions may be formulated for surface footings with a simple geometries, numerical analysis is required in the case of flexible embedded foundations with complex geometry. Thus, in the present analysis of suction caissons for offshore wind turbines, a coupled boundary element/finite element model is applied. The Finite Element Method (FEM) is very useful for the analysis of structure with local inhomogeneities and complex geometries. However, only a finite region can be discretized. Hence, at the artificial boundaries of the unbounded domain, e.g. soil, transmitting boundary conditions must be applied as suggested by Higdon (1990), Higdon (1992) and (Krenk 2002). Numerous

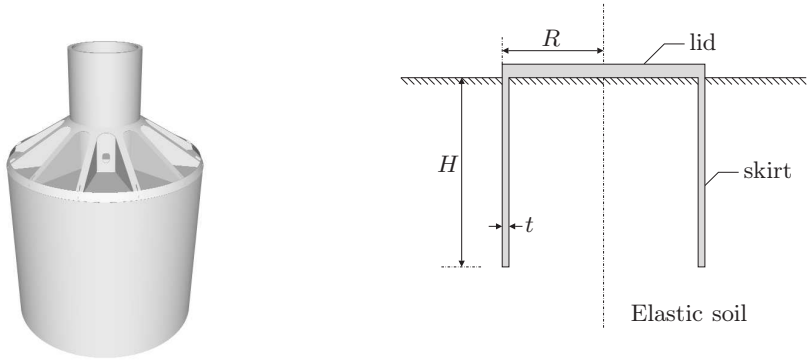

(a) (b)

Figure 1.1: Image (a) and geometry (b) of the suction caisson.

concepts, including the Scaled Boundary Finite Element Method are presented by Wolf and Song (1996), and Andersen (2002) gave a brief overview of different solutions techniques. However, in the present analysis, wave radiation into the subsoil is ensured by a coupling with the boundary element method. Since the full-space fundamental solution is utilized, both the soil–foundation interface and the free soil surface must be discretized. A smaller numerical model, i.e. a model with fewer degrees of freedom, may be obtained with the use of other types of solutions, e.g. half-space solutions. However, this comes at the cost that the fundamental solution can be very complicated, and often a closed-form solution cannot be found. Furthermore, cavities in a half-space are known to give rise to spurious modes of vibration when the half-space solution is applied (Pyl et al. 2004). This is not the case for the full-space Green's function. The work within the boundary element formulation of dynamic soil–structure interaction has been reported by, for example, Domínguez (1993), Domínguez (2003), Beskos (1987) and Beskos (1997).

1.3 Boundary element/finite element formulation

The dynamic stiffness of the suction caissons is evaluated by means of the dynamic three-dimensional coupled Boundary Element Method/Finite Element Method program BEASTS by Andersen and Jones (2001a). The boundary element part of BEASTS is an extension of the theory presented by Domínguez (1993), which has been modified to account for open domains and to allow a coupling with finite elements, see Andersen and Jones (2001b) for details.

1.3.1 Boundary element formulation

Let $\mathbf{x}$ define a point in the three-dimensional Cartesian space and let ω denote the cyclic frequency. The governing equation of motion for a three-dimensional body Ω in the

frequency domain is then given by

$$\frac{\partial \sigma_{ij}(\mathbf{x},\omega)}{\partial x_j} + \rho B_i(\mathbf{x},\omega) + \omega^2 \rho U_i(\mathbf{x},\omega) = 0, \qquad \mathbf{x} \in \Omega, \tag{1.1}$$

where summation is carried out over repeated indices. $U_i(\mathbf{x},\omega)$ (i=1,2,3) and $\sigma_{ij}(\mathbf{x},\omega)$ (j=1,2,3) are the complex amplitudes of the displacement field and the stresses, respectively. The latter may be computed from the displacements by the constitutive relation. Further, $\rho B_i(\mathbf{x},\omega)$ are the body forces. The boundary conditions on the surface Γ of the body Ω are:

$$\left.\begin{array}{ll} U_i(\mathbf{x},\omega) = \hat{U}_i(\mathbf{x},\omega) & \text{for} \quad \mathbf{x} \in \Gamma_U \\ P_i(\mathbf{x},\omega) = \hat{P}_i(\mathbf{x},\omega) & \text{for} \quad \mathbf{x} \in \Gamma_P \end{array}\right\}, \quad \Gamma = \Gamma_U \cup \Gamma_P,\ \Gamma_U \cap \Gamma_P = \emptyset, \tag{1.2}$$

where the displacement amplitude $U_i(\mathbf{x},\omega)$ is given on one part of the boundary, Γ_U, and the surface traction $P_i(\mathbf{x},\omega) = \sigma_{ij}(\mathbf{x},\omega)\, n_j(\mathbf{x})$ is given on the remaining part of the boundary, Γ_P. Here $n_j(\mathbf{x})$ are the components of the outward unit normal to the surface. To obtain the boundary element formulation of Equation (1.1), a second state $U^*_{il}(\mathbf{x},\omega;\boldsymbol{\xi})$ is identified as the fundamental solution to the equation of motion

$$\frac{\partial \sigma^*_{ijl}(\mathbf{x},\omega;\boldsymbol{\xi})}{\partial x_j} + \rho\delta(\mathbf{x}-\boldsymbol{\xi})\,\delta_{il} + \omega^2 \rho U^*_{il}(\mathbf{x},\omega;\boldsymbol{\xi}) = 0, \tag{1.3}$$

where $\delta(\mathbf{x}-\boldsymbol{\xi})$ is the Dirac delta function in vector form and δ_{il} is the Kronecker delta. It should be noted that the Green's function $U^*_{il}(\mathbf{x},\omega;\boldsymbol{\xi})$ represents a 3×3 matrix, i.e. there are three displacement components at the receiver point $\mathbf{x}$ for each direction l of the load applied at the source point $\boldsymbol{\xi}$. In three dimensions, $U^*_{il}(\mathbf{x},\omega;\boldsymbol{\xi})$ has a singularity of the order $1/r$, whereas the corresponding stress field $\sigma^*_{ijl}(\mathbf{x},\omega;\boldsymbol{\xi})$ has a singularity of the order $1/r^2$.

The fundamental solution is based on wave propagation in the full space and therefore only represents body waves emanating from the source, i.e. dilatation and shear waves with phase velocities c_P and c_S, respectively. The velocities c_P and c_S are given as

$$c_P = \sqrt{\frac{\lambda + 2G}{\rho}}, \quad c_S = \sqrt{\frac{G}{\rho}}, \tag{1.4}$$

where λ and G are the *Lamé constants* of the material, and ρ is the mass density. The Lamé constants λ and G can be written in terms of Young's modulus E and Poisson's ratio ν by the following relations:

$$G = \frac{E}{2(1+\nu)}, \qquad \lambda = \frac{\nu E}{(1+\nu)(1-2\nu)} \tag{1.5}$$

Material damping is introduced by a complex Young's modulus E^*, resulting in complex Lamé constants. The complex Young's modulus E^* is given by

$$E^* = E(1 + \mathrm{i}\eta), \tag{1.6}$$

where η is the loss factor of the material and $\mathrm{i} = \sqrt{-1}$ is the imaginary unit. Note that the loss factor is assumed to be constant for all frequencies, i.e. hysteretic damping is assumed.

The fundamental solution is applied as a weight function in the weak formulation of the equation of motion (1.1) for the physical field and vice versa. After some manipulations, and disregarding body forces in the interior of the domain, Somigliana's identity is derived:

$$C_{il}(\mathbf{x})\, U_l(\mathbf{x},\omega) + \int_\Gamma P^*_{il}(\mathbf{x},\omega;\boldsymbol{\xi})\, U_l(\boldsymbol{\xi},\omega,)\, \mathrm{d}\Gamma_{\boldsymbol{\xi}} = \int_\Gamma U^*_{il}(\mathbf{x},\omega;\boldsymbol{\xi})\, P_l(\boldsymbol{\xi},\omega,)\, \mathrm{d}\Gamma_{\boldsymbol{\xi}} \qquad (1.7)$$

Here $P^*_{il}(\mathbf{x},\omega;\boldsymbol{\xi})$ is the surface traction related to the Green's function $U^*_{il}(\mathbf{x},\omega;\boldsymbol{\xi})$. $C_{il}(\mathbf{x})$ is a doubly indexed scalar that only depends on the geometry of the surface Γ. In particular, $C_{il}(\mathbf{x}) = 1/2\delta_{il}$ on a smooth part of the boundary Γ and $C_{il}(\mathbf{x}) = \delta_{il}$ inside the body Ω. A detailed derivation of (1.7) and properties of $C_{il}(\mathbf{x})$ are given in (Andersen 2002; Domínguez 1993).

In order to evaluate the boundary integral equations in (1.7) for a point $\mathbf{x}$ on the boundary, the surface is discretized into a finite number of boundary elements. The boundary integral equation can then be solved numerically for any point $\mathbf{x}$ on the boundary. The boundary can be discretized by different types of elements with varying order of integration. In the present study, quadrilateral elements with quadratic interpolation are employed, due to the fact that nine-noded boundary elements are superior in performance and convergence compared to elements with constant or linear interpolation (Andersen 2002).

To obtain the BE formulation, the state variable fields on the boundary are discretized. $\mathbf{U}_j(\mathbf{x})$ and $\mathbf{P}_j(\mathbf{x})$ be the vectors storing the displacements and tractions at the N_j nodes in element j. The displacement and traction fields over the element surface Γ_j then become

$$\mathbf{U}(\mathbf{x},\omega) = \boldsymbol{\Phi}_j(\mathbf{x})\, \mathbf{U}_j(\omega)\,, \quad \mathbf{P}(\mathbf{x},\omega) = \boldsymbol{\Phi}_j(\mathbf{x})\, \mathbf{P}_j(\omega)\,, \qquad (1.8)$$

where $\boldsymbol{\Phi}_j(\mathbf{x})$ is a matrix storing the interpolation, or shape, functions for the element. This allows the unknown values of the state variables to be taken outside the integrals in Equation (1.7). Finally, the three-row matrices originating from Equation (1.7) for each of the observation points may be assembled into a single matrix equation for the entire BE domain,

$$\mathbf{H}(\omega)\, \mathbf{U}(\omega) = \mathbf{G}(\omega)\, \mathbf{P}(\omega)\,. \qquad (1.9)$$

Component $(i,\, k)$ of the matrices $\mathbf{H}(\omega)$ and $\mathbf{G}(\omega)$ stores the influence from degree-of-freedom k to degree-of-freedom i for the traction and the displacement, respectively, i.e. the integral terms on the left- and right-hand side of Equation (1.7). The geometric constants $C_{il}(\mathbf{x})$ are absorbed into the diagonal of $\mathbf{H}(\omega)$.

1.3.2 Coupling of FE and BE regions

The finite element (FE) region of the model is formulated by the equation of motion in the frequency domain (Andersen and Jones 2002):

$$\left(-\mathbf{M}\omega^2 + \mathrm{i}\mathbf{C} + \mathbf{K}\right)\mathbf{U} = \mathbf{K}_{FE}\mathbf{U} = \mathbf{F}, \qquad (1.10)$$

where $\mathbf{M}$, $\mathbf{C}$ and $\mathbf{K}$ are the mass, damping and stiffness matrices, respectively. $\mathbf{U}$ contains the nodal displacements and $\mathbf{F}$ the nodal forces. Hysteretic material damping is assumed, i.e. $\mathbf{C} = \eta\mathbf{K}$. Hence, the damping term is independent of the circular frequency ω.

In the subsequent analysis, the foundation consists of relatively thin structures (skirt) and the use of boundary elements in this region is inappropriate due to the singularities of the Green's functions. In these regions finite elements are used. In order to couple a BE domain formulated in terms of surface tractions with an FE region with loads applied in terms of nodal forces, a transformation matrix $\mathbf{T}$ is defined, such that $\mathbf{F} = \mathbf{TP}$. Here $\mathbf{F}$ is the vector of nodal forces equivalent to the tractions $\mathbf{P}$ applied on the surface of the domain. The transformation matrix only depends on the spatial interpolation functions, i.e. the shape functions, for the elements along the interaction boundary. Hence, $\mathbf{T}$ may be determined once and for all and applied in all analyses with a given model geometry. Subsequently, for each frequency the matrix

$$\mathbf{TG}^{-1}\mathbf{H} = \mathbf{K}_{BE} \tag{1.11}$$

defines an *equivalent dynamic stiffness matrix* for the boundary element domain. This operation turns the BE domain into a macro finite element. It should be noted that $\mathbf{K}_{BE}$ is a fully populated and asymmetrical matrix, as opposed to $\mathbf{K}_{FE}$ which is a sparsely populated, banded and symmetric matrix. For detailed discussion regarding the coupling between a BE and FE regions, see Andersen and Jones (2001b).

1.4 Static and dynamic stiffness formulation

A generalized massless axisymmetric foundation with a rigid base has six degrees of freedom: one vertical, two horizontal, two rocking and one torsional. The six degrees of freedom and the corresponding forces and moments are shown in Figure 1.2. For a harmonic excitation with the cyclic frequency ω, the dynamic stiffness matrix $\mathbf{S}$ is related to the vector of forces and moments $\mathbf{R}$ and the vector of displacements and rotations $\mathbf{U}$ as follows:

$$\mathbf{R} = \mathbf{SU} \tag{1.12}$$

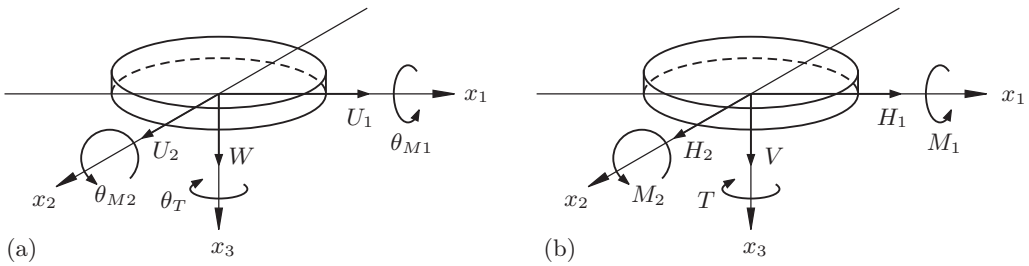

Figure 1.2: Degrees of freedom for a rigid surface footing: (a) displacements and rotations, and (b) forces and moments.

The component form of Equation (1.12) can be written as:

$$\begin{bmatrix} V/G_sR^2 \\ H_1/G_sR^2 \\ H_2/G_sR^2 \\ T/G_sR^3 \\ M_1/G_sR^3 \\ M_2/G_sR^3 \end{bmatrix} = \begin{bmatrix} S_{VV} & 0 & 0 & 0 & 0 & 0 \\ 0 & S_{HH} & 0 & 0 & 0 & -S_{MH} \\ 0 & 0 & S_{HH} & 0 & S_{MH} & 0 \\ 0 & 0 & 0 & S_{TT} & 0 & 0 \\ 0 & 0 & S_{MH} & 0 & S_{MM} & 0 \\ 0 & -S_{MH} & 0 & 0 & 0 & S_{MM} \end{bmatrix} \begin{bmatrix} W/R \\ U_1/R \\ U_2/R \\ \theta_T \\ \theta_{M1} \\ \theta_{M2} \end{bmatrix} \tag{1.13}$$

where R is the radius of the foundation and G_s is the shear modulus of the soil. The components in $\mathbf{S}$ are functions of the cyclic frequency ω and Poisson's ratio of the soil ν_s. The nonzero terms in $\mathbf{S}$ can be written as:

$$S_{ij}(a_0) = K_{ij}^0 \left[k_{ij}(a_0) + \mathrm{i}a_0 c_{ij}(a_0)\right], \qquad (i,j = H,M,T,V), \tag{1.14}$$

where K_{ij}^0 is the static value of ijth stiffness component, whereas k_{ij} and c_{ij} are the dynamic stiffness and damping coefficients, respectively. Furthermore, $a_0 = \omega R/c_S$ is the dimensionless frequency where c_S is the shear wave velocity of the soil. The real part of Equation (1.14) is related to the stiffness and inertia properties of the soil–structure system, whereas the imaginary part describes the damping of the system. For a soil without material dissipation, c_{ij} reflects the geometric damping, i.e. the radiation of waves into the subsoil.

In some situations it is useful to examine the magnitude and phase angle of Equation (1.14) in addition to the real and imaginary parts of the dynamic stiffness. The magnitude (complex modulus) and the phase angle ϕ_{ij} of S_{ij} are given by

$$|S_{ij}| = K_{ij}^0 \sqrt{(k_{ij})^2 + (a_0 c_{ij})^2}, \quad \phi_{ij} = \arctan\left(\frac{a_0 c_{ij}}{k_{ij}}\right). \tag{1.15}$$

1.5 Benchmark tests

The coupled BE/FE model of the suction caisson has been tested and compared with known analytical and numerical results. The first comparison concerns the capability of determining the static stiffness of the suction caisson by the BE/FE formulation. In the second comparison the BE/FE model of the suction caisson has been used to reproduce the vertical dynamic stiffness of a surface foundation by setting the skirt properties equal to the properties of the surrounding soil.

1.5.1 Verification of the vertical static stiffness

The vertical static stiffness K_{VV}^0 corresponds to the stiffness of the soil-foundation system without any inertial or material dissipation effects. The vertical static stiffness coefficient has been determined by means of a static finite element analysis in ABAQUS (Abaqus 2003). These static results have been used as convergence criteria for the element mesh size in the subsequent boundary element analyses of the dynamic stiffness. The reason for using the static stiffness as convergence criteria is that the shape of the impedance (location of peaks as function of frequency) converges with a relatively coarse mesh,

compared to the actual magnitude of the impedance. Surprisingly, it turns out that the magnitude of the impedance is the critical convergence parameter. The static stiffness from the FE/BE models are estimated for a very low excitation frequency, $a_0 = 0.01$, where the inertial effects are negligible.

ABAQUS model

The static three-dimensional ABAQUS model of the suction caisson consists of a foundation and near-field soil domain modelled by second order finite elements and a far field soil domain modeled by infinite elements. The skirt of the suction caisson is flexible, considering the fact that the skirt thickness is small compared to the height or diameter of the foundation. The lid is assumed to be rigid. The lid is modelled as a solid finite element section with a thickness of one meter and the same material properties as the skirt. The ABAQUS model contains approximately 200,000 degrees of freedom and the runtime is approximately 1 hour per stiffness coefficient on a 2.0 GHz P4 laptop computer. The BE/FE model is described in the next subsection.

Results

The non-dimensional values of K^0_{VV} are given for three different cases:

Different skirt lengths: – The static stiffness K^0_{VV} is given for various ratios between the foundation diameter D and the length of the skirt H in Table 1.1. The soil properties are $G_s = 1$ MPa and $\nu_s = 1/3$.

Different Poisson's ratios: – The variation of K^0_{VV} with respect to Poisson's Ratio is shown in Table 1.1. H/D=1 and $G_s = 1$ MPa.

Varying soil stiffness: – K^0_{VV} is given for different values of the shear modulus G_s in the soil in Table 1.1. H/D=1 and ν_s is 1/3.

The data are shown for fixed material properties of the foundation ($E_f = 210$ GPa, $\nu_f = 0.25$). The foundation radius is $R = 5$ m and the skirt thickness is $t = 50$ mm. In general there is a good agreement between the values of K^0_{VV} computed by FE and BE/FE when it is taken into account that K^0_{VV} has been calculated with two different methods of analysis and discretization. There is a tendency of increasing deviations with decreasing Poisson's ratio and increasing skirt length. It should be noted that the static vertical stiffness for low values of G_s (0.1 and 1.0 MPa) is equivalent to the stiffness of a suction caisson with rigid skirts, whereas high values of G_s (approaching the shear modulus of the skirts) correspond to the behaviour of a rigid base surface foundation. The results agree with the work by Doherty and Deeks (2003) and Doherty et al. (2005) who employed the scaled boundary finite element method to analyse the static stiffness of suction caissons embedded in non-homogeneous elastic soil.

1.5.2 Reproduction of the vertical dynamic stiffness of a surface footing

Next, the FE/BE model of the suction caisson ($H/D = 1$) is tested against known analytical and numerical results for the vertical dynamic stiffness of a surface footing.

Table 1.1: Vertical static stiffness

		K^0_{VV} FE	K^0_{VV} FE/BE	Deviation
$H/D =$	1/4	7.25	7.39	−1.88 %
	1	10.70	10.87	−1.60 %
	2	14.61	14.99	−2.53 %
$\nu_s =$	0.1	9.20	9.72	−5.38 %
	0.2	9.74	10.13	−3.85 %
	0.333	10.70	10.87	−1.60 %
	0.4	11.32	11.39	−0.60 %
	0.495	12.89	12.68	+1.64 %
$G_s =$	10^5 Pa	10.73	10.91	−1.65 %
	10^6 Pa	10.70	10.87	−1.60 %
	10^7 Pa	10.65	10.48	+1.58 %
	10^8 Pa	10.03	10.19	−1.62 %
	10^9 Pa	7.85	8.01	−2.03 %

In the BE/FE model of the suction caisson, the skirt has been given material properties equal to the properties of the surrounding soil. The model of the suction caisson should then be able to reproduce the results obtained for a massless surface footing. The results obtained from the suction caisson model are compared with a BE/FE analysis of a surface footing and a known analytical solution. The analytical solution given by Veletsos and Tang (1987) is based on a perfect elastic half-space with Poisson's ratio equal to 1/3, and relaxed boundary conditions under the foundation are assumed, corresponding to the condition of 'smooth' contact.

Boundary Element/Finite Element models

Due to symmetry only half the foundation is included. In the finite element region only half the model needs to be analysed when a plane of symmetric exists. The degrees of freedom in the plane of symmetry are simply eliminated in the system of equations in order to satisfy the conditions at the interface between the modelled and non-modelled part. The procedure for introducing a plane of symmetry in the BE region is more complex, and will not be given here. The procedure for BE analysis of problems with geometrical symmetry is discussed in details by Andersen and Jones (2001b).

The BE/FE model of the surface footing contains a massless circular foundation with the radius $R = 5$ m. The foundation is modelled by 40 quadrilateral finite elements employing quadratic interpolation. The thickness (height) of the foundation is one meter. The soil is discretized into a total of 152 boundary elements with quadratic interpolation. The model is illustrated in Figure 1.3a.

The BE/FE model of the suction caisson consists of four sections: a massless finite element section that forms the top of the foundation where the load is applied, a finite element section of the skirts, a boundary element domain inside the skirts and, finally, a boundary element domain outside the skirts that also forms the free surface. The skirt

of the suction caisson is considered flexible, and the lid is assumed to be rigid. The lid is modelled as a solid finite element section with a thickness of one meter. Again, quadratic interpolation is employed. The models of the suction caisson and the subsoil contain approx. 100 finite elements and 350 boundary elements. The model is illustrated in Figure 1.3b. For both numerical models, the soil is linear elastic with $G_s = 1$ MPa, $\nu_s = 1/3$ and $\rho_s = 1000$ kg/m^3. The material of the surface foundation and the lid of the suction caisson is linear elastic with $G_s = 10^6$ MPa, $\nu_s = 1/3$ and $\rho_s = 0$ kg/m^3. The connection between soil and foundation corresponds to the condition of 'rough' contact since the foundation and the surrounding soil have common degrees of freedom.

The mesh of the free surface for the surface foundation has been truncated at a distance of 15 m (3 times radius R) from the centre of the footing, based on convergence studies. Regarding the suction caisson ($H/D = 1$), the mesh of the free surface is truncated at a distance of 30 m (6 times radius R) from the centre of the foundation. The truncation distance for the models of the suction caisson depends on the skirt embedment. Convergence studies for the worst case ($H/D = 2$) suggested a truncation distance of 30 m from the centre of the foundation. This length has been used for all the BE/FE analyses of the suction caisson, regardless of embedment depth of the skirt. Adaptive meshing could possibly improve the accuracy versus the number of degrees of freedom, but this facility is currently not available in the BE/FE software.

For a given excitation frequency a vertical load equal to 1 N is applied in the centre on top of the foundations and the complex displacements are computed. The complex vertical dynamic stiffness is then determined from the load and the displacement response. Note that load control has been used to generate the stiffness values. Displacement control would be more appropriate, but this feature is currently not available in the BE/FE software.

The models contains approximately 1000 (surface model) to 3000 (suction caisson model) degrees of freedom and the runtime is approximately 5 to 30 minutes for each excitation frequency on a 2.0 GHz P4 laptop computer.

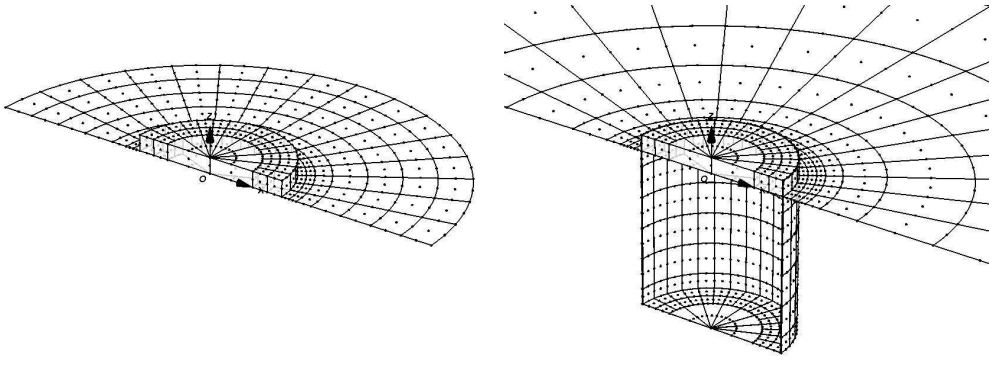

(a) (b)

Figure 1.3: BE/FE models of (a) surface foundation and (b) suction caisson ($H/D = 1$).

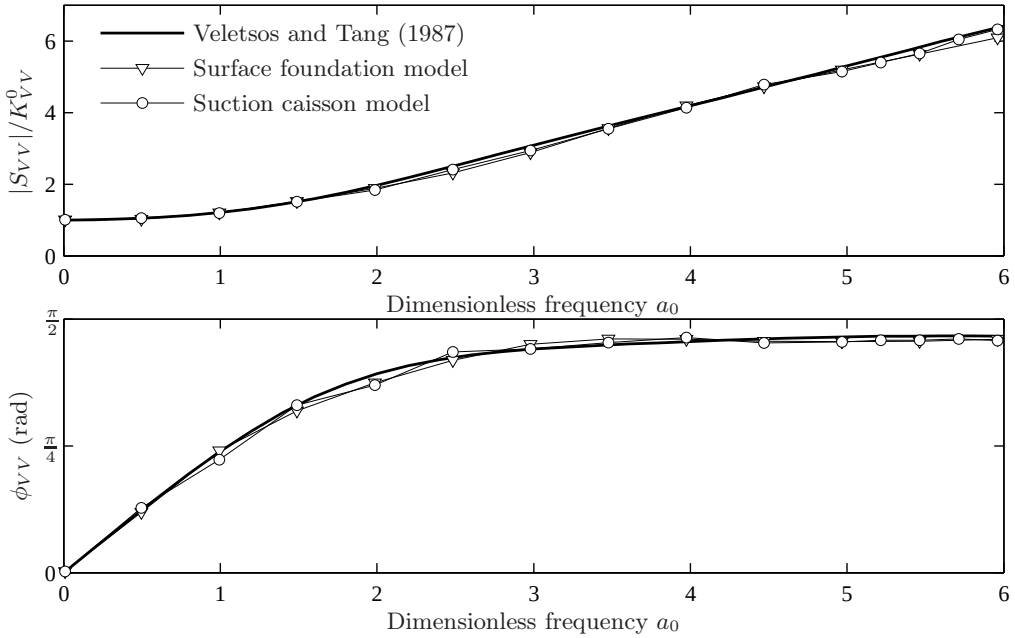

Figure 1.4: Vertical dynamic stiffness for a surface foundation calculated by two different BE/FE models. The numerical results are compared with a known analytical solution.

Results

The BE/FE models have been utilized for 13 excitation frequencies in the range $a_0 \in]0;6]$. The results obtained from the numerical models are given in Figure 1.4 together with the known analytical solution reported by Veletsos and Tang (1987). The upper plot shows the normalized magnitude $|S_{VV}|/K^0_{VV}$, and the phase angle ϕ_{VV} is shown in the lower plot. First of all, the numerical models are able to reproduce the overall pattern of the frequency dependent stiffness of the analytical solution, when it is considered that the analytical solution by Veletsos and Tang (1987) is based on relaxed boundary conditions and the boundary element solutions corresponds to welded, or rough, contact. The same type of results have been reported by Alarcon et al. (1989). The results from the suction caisson model with 'soil skirts' match the results of the surface foundation model quite well, and it is concluded that the model of the suction caisson is able to reproduce the frequency dependent behaviour of a surface foundation without introducing errors due to the complexity of the model (two boundary element domains separated by a thin finite element structure).

1.6 Dynamic stiffness for vertical vibrations

In this section the dynamic stiffness is investigated for several different combinations of the mechanical properties of the soil–foundation system. The first case concerns the effects of Poisson's ratio on the stiffness. In the second analysis the flexibility of the soil–foundation system is investigated for different ratios between the soil and the foundation stiffness. The third case is the variation of the stiffness due to a change in the skirt length. The first two analyses are carried out for the frequency range $a_0 \in]0;6]$, whereas the third analysis is extended to a larger frequency range $a_0 \in]0;12]$.

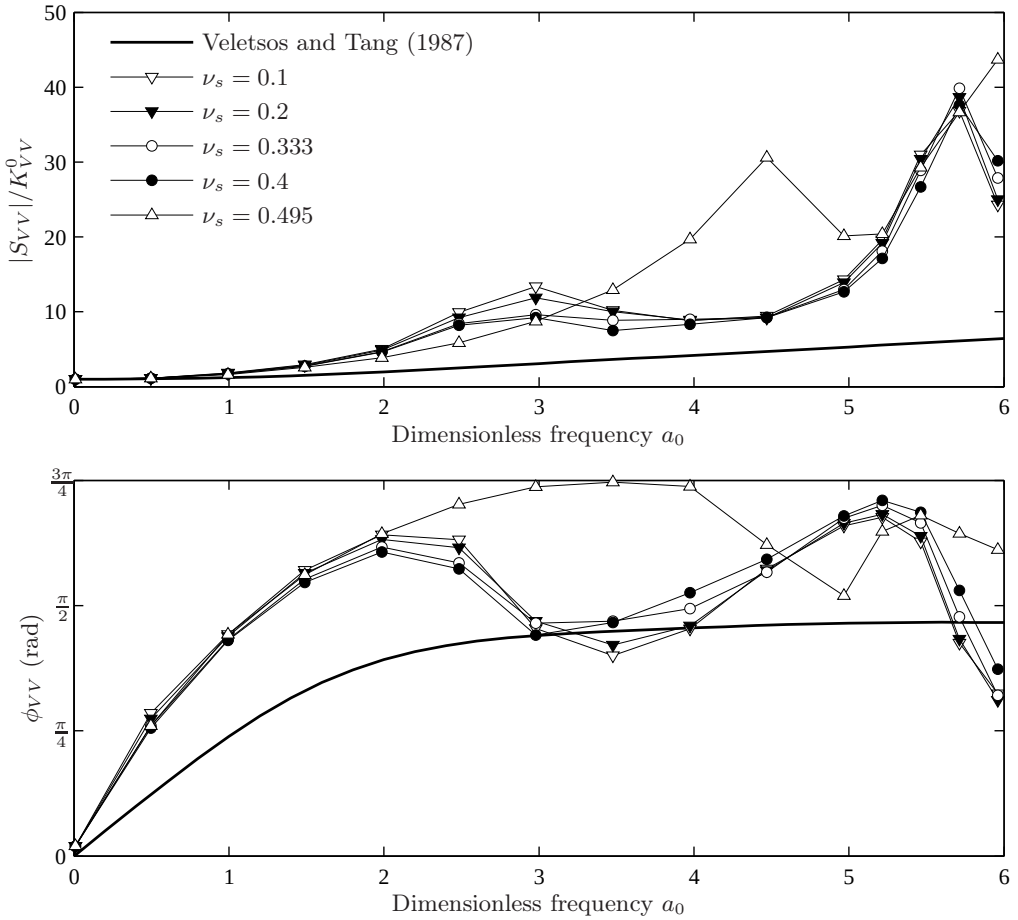

Figure 1.5: Vertical dynamic stiffness: variation of Poisson's ratio. $H/D = 1$, $G_s = 1.0$ MPa and $\eta_s = 5\%$.

1.6.1 Vertical dynamic stiffness—variation of Poisson's ratio

The dynamic stiffness for different Poisson's ratios is presented in this section. The skirt length is fixed ($H/D = 1$). The model properties are $G_s = 1.0$ MPa, $\rho_s = 1000$ kg/m^3, $\eta_s = 5$ %, $E_f = 210$ GPa, $\nu_f = 0.25$, $\eta_f = 2$ % and $t = 50$ mm. In order to model a massless foundation $\rho_f = 0$ for the lid of the caisson and $\rho_f = \rho_s$ for the skirt. In Figure 1.5, the results are shown for 5 different values of Poisson's ratio for the frequency range $a_0 \in]0;6]$. The dynamic stiffness is relatively insensitive to variations in ν_s in the range from 0.1 to 0.4. When ν_s approaches 0.5, the dynamic behaviour changes significantly. The main reason for the change in the dynamic behaviour for ν_s close to 0.5 is the fact that $c_P/c_S \in [\sqrt{2};2]$ for $\nu_s \in [0;1/3]$, whereas $c_P/c_S \to \infty$ for $\nu_s \to 0.5$. Thus, for constant G_s the P-wave speed becomes infinite for $\nu_s \to 0.5$. Note that it is possible to solve the BE system for $\nu_s = 0.5$ by reordering the fundamental solution, however, here the range in Poisson's ratio is thought to cover fully drained ($\nu_s = 0.1-0.2$) to undrained ($\nu_s = 0.495$) conditions.

1.6.2 Vertical dynamic stiffness—variation of soil stiffness

The influence of the ratio between the stiffness of the soil and the stiffness of the structure is evident from the analysis of the static stiffness, see Table 1.1. The influence on the dynamic behaviour is shown in Figure 1.6 for the frequency range $a_0 \in]0;6]$. The fixed model properties are $H/D = 1$, $\nu_s = 1/3$, $\rho_s = 1000$ kg/m^3, $\eta_s = 5$ %, $E_f = 210$ GPa, $\nu_f = 0.25$, $\eta_f = 2$ % and $t = 50$ mm. To model a massless foundation $\rho_f = 0$ for the lid of the caisson and $\rho_f = \rho_s$ for the skirt.

The shape of the curve for high values of G_s (1000 MPa) is approaching the shape of the frequency dependent behaviour of the surface foundation. When G_s decreases, the local oscillations become more distinct and the influence of the skirt flexibility vanishes, i.e. the caisson reacts as a rigid foundation. Rigid behaviour can be assumed for $G_s \leq 1.0$ MPa.

1.6.3 Vertical dynamic stiffness—high-frequency behaviour

The variation of the dynamic stiffness due to a change in the skirt length H is presented in the following. The BE/FE models for the analysis are similar to the model shown in Figure 1.3b. The model properties are $G_s = 1$ MPa, $\nu_s = 1/3$, $\rho_s = 1000$ kg/m^3, $\eta_s = 5$ %, $E_f = 210$ GPa, $\nu_f = 0.25$, $\eta_f = 2$ % and $t = 50$ mm. . Note that $\rho_f = 0$ for the lid of the caisson and $\rho_f = \rho_s$ for the skirt. In order to get a picture of the high frequency behaviour of the suction caisson, the analyses have been performed for the frequency range $a_0 \in]0;12]$. The components of the vertical dynamic stiffness for H/D=1/4, 1 and 2 are shown in Figure 1.7.

The vertical dynamic stiffness of the caisson with a relatively small embedment depth ($H/D = 1/4$) varies smoothly with the frequency, whereas the magnitude for $H/D = 1$ and 2 is characterized by distinct peaks, and it can be observed that the magnitude of dynamic stiffness overall increases with the skirt length.

The normalized magnitude of the impedance is characterized by repeated oscillations with local extremes. However, the average dynamic stiffness, measured over a wide range

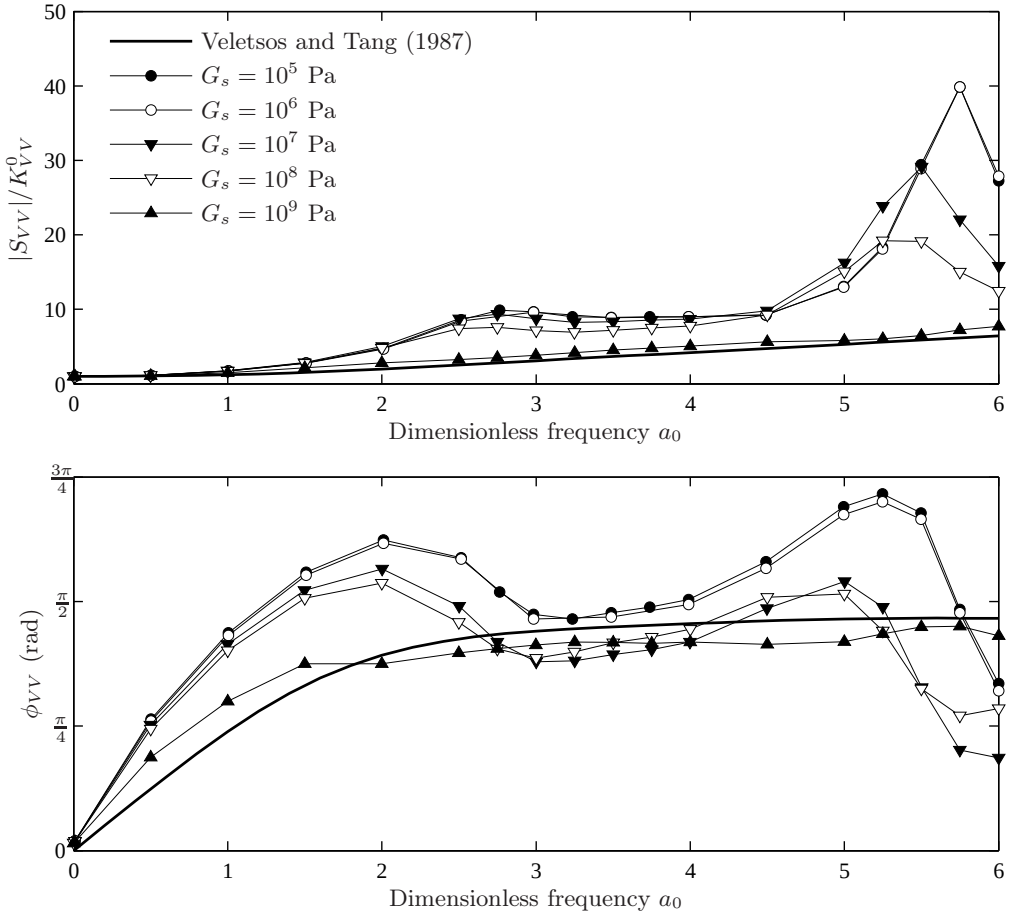

Figure 1.6: Vertical dynamic stiffness: variation of soil stiffness. $H/D = 1$, $\nu_s = 1/3$ and $\eta_s = 5\%$.

of frequencies, appears to be increasing monotonously with increasing frequency, similar to the situation for the surface footing in Figure 1.7.

I order to formulate the high-frequency behaviour of foundations by lumped-parameter models (see Ibsen and Liingaard (2006b)) a dashpot is used to describe the high-frequency impedance. The high-frequency behaviour is characterized by a phase angle approaching $\pi/2$ for $a_0 \to \infty$ and a linear relation that passes through origo in a frequency vs. magnitude diagram. The slope of the curve is equal to a limiting damping parameter C_{VV}^{∞} that describes the impedance for $a_0 \to \infty$, which in the case of the surface footing is given by

$$C_{VV}^{\infty} = \rho_s c_P A_b, \tag{1.16}$$

where A_b is the area of the base of the foundation. It should be noted that C_{VV}^{∞} in Equation (1.16) is highly sensitive to ν_s due to the fact that c_P enters the equation. For

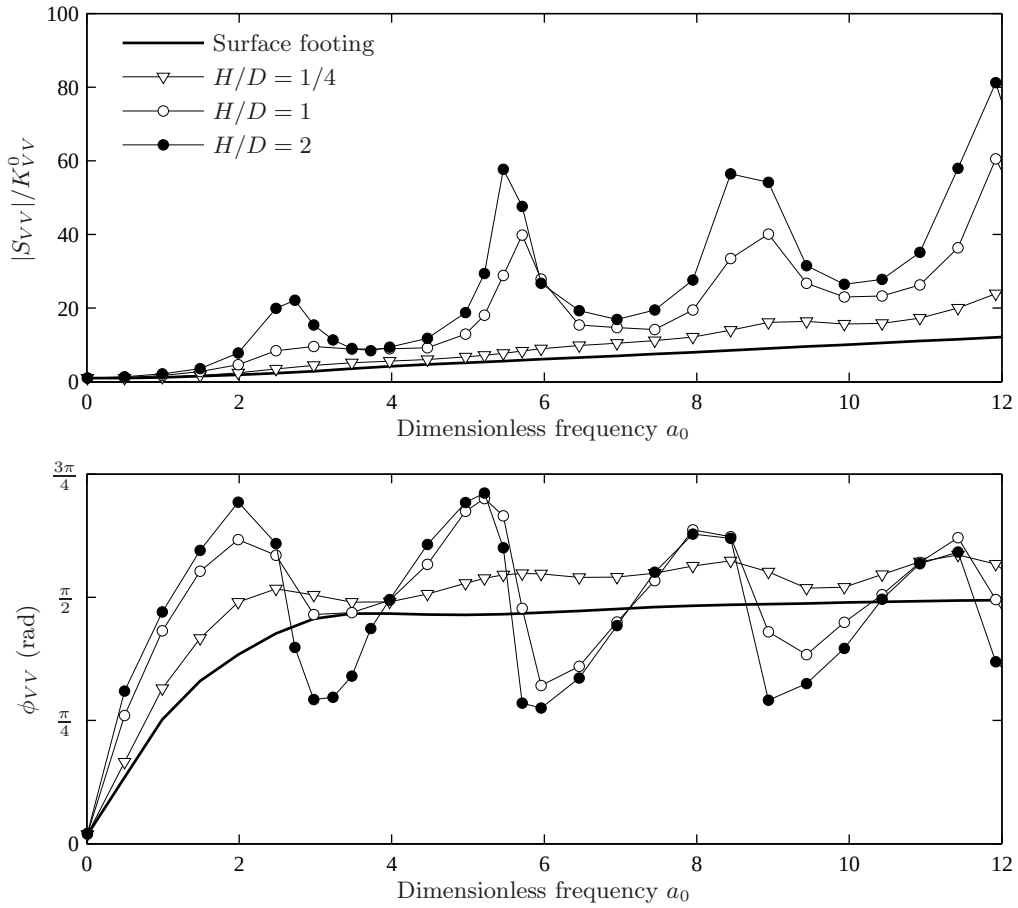

Figure 1.7: Vertical dynamic stiffness: high frequency behaviour. $G_s = 1.0$ MPa, $\nu_s = 1/3$ and $\eta_s = 5\%$.

that reason c_P may be inappropriate, and Gazetas and Dobry (1984) suggest the use of *Lysmer's analog* 'wave velocity' c_{La}=$3.4c_S/\pi(1-\nu_s)$. Wolf (1994) suggests another approach where c_P for $\nu_s \in [1/3;0.5]$ is constant, and equal to c_P at $\nu_s = 1/3$.

At high frequencies the wavelengths are small compared with the dimensions of the source (or the vibrating surface). Thus, the soil immediately below the vibrating surface of a smooth surface footing is only exposed to P-waves. However, the skirts of the suction caisson generate additional S-waves due to a vertical high-frequency excitation. For that reason, the limiting damping parameter C^∞_{VV} of the suction caisson consists of two contributions: one from the vibration of the lid and one originating from the vibration of the skirt. C^∞_{VV} of the suction caisson is then given by

$$C^\infty_{VV} = \rho_s c_P A_{lid} + 2\rho_s c_S A_{skirt}, \tag{1.17}$$

where A_{lid} and A_{skirt} are the vibrating surface areas of the lid and the skirt, respectively.

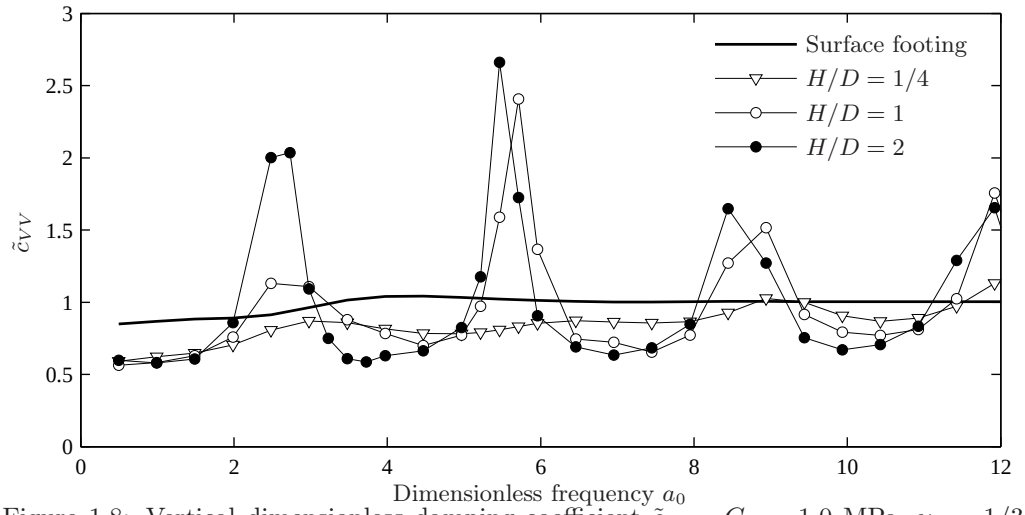

Figure 1.8: Vertical dimensionless damping coefficient $\tilde{c}_{VV}$. $G_s = 1.0$ MPa, $\nu_s = 1/3$ and $\eta_s = 5\%$.

Note that S-waves are generated both inside and outside the skirt, hence the factor '2' in the latter contribution in Equation (1.17). The discussion of the proper choice of c_P also applies here.

In order to verify that the high-frequency behaviour of the suction caisson, described by (1.17), the damping term c_{VV} in Equation (1.14) is compared with C^{∞}_{VV}. This is carried out by means of the dimensionless damping coefficient $\tilde{c}_{VV}$, given by

$$\tilde{c}_{VV} = \frac{\frac{R}{c_S} c_{VV}\left(a_0\right)}{C^{\infty}_{VV}}. \tag{1.18}$$

At high frequencies $\tilde{c}_{VV}$ should tend towards unity if the expressions in Equations (1.16) and (1.17) hold true (Dobry and Gazetas 1986). In Figure 1.8 the dimensionless damping coefficient $\tilde{c}_{VV}$ is plotted for the suction caisson data together with the results for a surface footing. It is evident that the dimensionless damping coefficient of the surface footing tends towards unity as the frequency increases. With respect to the suction caisson the problem is somewhat more complex. The high-frequency behaviour contains an infinite number of resonance peaks as $a_0 \to \infty$. However, this behaviour cannot be quantified by one single damping parameter, so the coefficient in Equation 1.17 reflects the average behaviour of high-frequency vibrations. It should be emphasized that the purpose of determining the high-frequency dashpot parameters in Equations (1.16) and (1.17) is to control the lumped-parameter model approximation of the high-frequency vibrations. Note that c_P at $\nu_s = 1/3$ has been used in Equations (1.16) and (1.17).

1.7 Discussion

There are several observations associated with the oscillations of the impedance of the suction caissons:

- The peaks of the normalized magnitude are located at phase angles equal to $\pi/2$.
- The distance between the peaks is approximately $\Delta a_0 = 3.0$ - 3.5.
- The amplitude of the peaks increases significantly with skirt length.

However, the appearance of distinct peaks in the magnitude of the stiffness around certain frequencies cannot be explained by the variation of skirt length, Poisson's ratio and the flexibility of the skirt. The fact that the oscillations are repeated for equal distances in frequency suggests that the phenomenon is due to wave interference in the soil inside the suction caisson. Since the amplitude of the peaks significantly increases with skirt length, it seems reasonable to examine the axial impedance of an infinite cylinder, in order to study the wave interference inside the caisson.

The dynamic stiffness per unit length of an infinite cylinder subjected to dynamic vertical excitation in the axial direction is shown in Figure 1.9. The dynamic stiffness is computed for η_s=0.00, 0.05 and 0.10, and the data are represented by the normalized magnitude and the phase angle. The slope of the dashed line in Figure 1.9 is equal to the limiting damping parameter C_{zz}^{∞} per unit length of the infinite cylinder. Note that the vertical motion of the infinitely long cylinder only generates S-waves, i.e. there is no contribution of P-waves. The solution for the impedance of the infinite cylinder subjected to dynamic vertical excitation in the axial direction is given in Appendix A.

The similarities of the impedance in Figure 1.7 and 1.9 are remarkable. However, the normalized magnitudes are not to scale, but the patterns of the magnitude and phase angle of the suction caissons ($H \geq 1$) are equivalent to those of the infinite cylinder for $\eta_s = 0.05$. The closed-form solution to the vertical dynamic stiffness $S_{VV}(\omega)$ of the infinite cylinder is given by

$$S_{VV}(\omega) = \frac{K_{VV}^0}{RJ_0(k_S R)\, K_0(\mathrm{i}k_S R)}, \quad K_{VV}^0 = 2\pi R G_s, \tag{1.19}$$

where J_0 is the Bessel function of the first kind and order 0, K_0 is the modified Bessel function of the second kind and order 0, whereas $k_S = \omega/c_S$ is the wavenumber of S-waves. Recall that G_s is the shear modulus of the soil. Note that Equation (1.19) is given by Equations (A.7) and (A.11) in Appendix A. As reported by Kitahara (1984), $J_0(k_S R)$ has a number of zeros for $\eta_s = 0$ and $k_S > 0$. At the corresponding cyclic frequencies, $S_{VV}(\omega)$ becomes singular and the stiffness becomes infinite. These anti-resonance frequencies are marked in Figure 1.9 by the vertical lines with the dash-dot signature. The distance between the lines tends towards π for $\omega \to \infty$. Thus, the nth anti-resonance mode occurs at the non-dimensional frequency $a_0 \to \pi(n - 1/4)$ for $n \to \infty$.

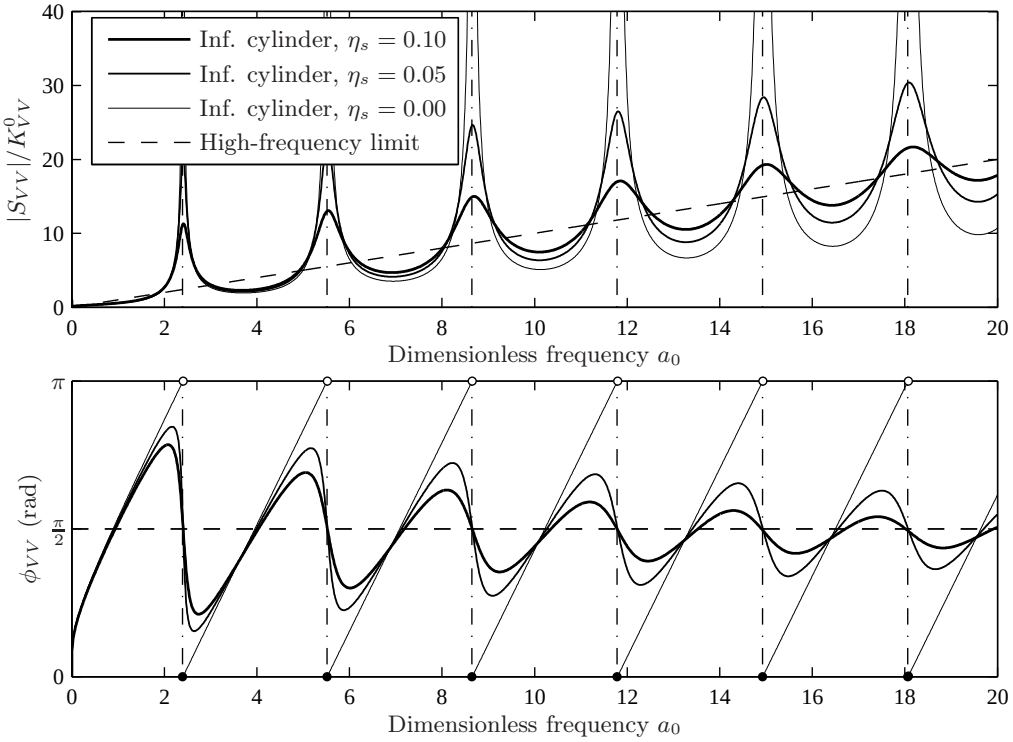

Figure 1.9: Solution for an infinite cylinder subjected to dynamic vertical excitation in the axial direction.

1.8 Conclusion

In this report the vertical dynamic soil–structure interaction of the suction caisson foundations for offshore wind turbines has been evaluated by means of a dynamic three-dimensional coupled Boundary Element/Finite Element model.

Benchmark tests have been performed to determine the capability of estimating the vertical static stiffness of the suction caisson by the BE/FE formulation, and there is good agreement between the estimation of K^0_{VV} by FE and BE/FE. Furthermore, the BE/FE model of the suction caisson has been used to reproduce the vertical dynamic stiffness of a surface footing. The results from the suction caisson model with 'soil skirts' match the results of the surface foundation model, and the model of the suction caisson is able to reproduce the frequency dependent behaviour of a surface foundation without introducing errors due to the complexity of the model.

The dynamic stiffness has been investigated for several different combinations of the mechanical properties of the soil–foundation system, and the following observations can be made:

- The vertical dynamic stiffness changes with the skirt length. For a relatively small embedment depth ($H/D = 1/4$) the impedance varies smoothly with the frequency,

whereas the impedance for $H/D = 1$ and 2 is characterized by distinct peaks.

- The dynamic stiffness is relatively insensitive to variations in ν_s in the range from 0.1 to 0.4. When ν_s approaches 0.5, the dynamic behaviour changes significantly due to the fact that $c_P/c_S \to \infty$ for $\nu_s \to 0.5$.
- The impedance for high values of G_s (1000 MPa) approaches the shape of the frequency dependent behaviour of the surface foundation. When G_s decreases, the local oscillations become more distinct and the influence of the skirt flexibility vanishes, i.e. the caisson reacts as a rigid foundation. Rigid behaviour can be assumed for $G_s \leq 1.0$ MPa.

Furthermore, the high-frequency behaviour of the suction has been investigated. Here, the main conclusions are:

- Generally the magnitude of the impedance increases with the skirt length.
- The normalized magnitude of the impedance is characterized by repeated oscillations with local extremes for $a_0 \in]0;12]$. However, the average dynamic stiffness appears to be increasing monotonously with increasing frequency, similar to the situation for of the surface footing.
- The phase angle for the suction caissons oscillate around $\pi/2$ for $a_0 > 4$, and it will eventually stabilize at higher frequencies.
- A limiting damping parameter C_{zz}^{∞} that describes the impedance for $a_0 \to \infty$ has been determined for applications involving lumped-parameter model approximation of the high-frequency vibrations.

The repeated oscillations in the impedance of the suction caisson are due to resonance and anti-resonance of the soil inside the suction caisson. This is concluded by comparing the vertical impedance characteristics of the suction caisson to those of an infinite cylinder subjected to dynamic vertical excitation in the axial direction.

This report has been focused on the analysis of the vertical component of the dynamic stiffness matrix $\mathbf{S}$ and the preliminary benchmark testing to ensure that the numerical model is valid and able to capture the dynamic behaviour of the suction caisson. The analysis of the coupled horizontal and moment loading and the torsional loading conditions will be examined in Ibsen and Liingaard (2006a).

Bibliography

Abaqus (2003). *ABAQUS—Version 6.4*. ABAQUS, Inc 2003, 1080 Main Street, Pawtucket, RI 02860-4847.

Alarcon, E., J. J. Cano, and J. Domínguez (1989). Boundary element approach to the dynamic stiffness functions of circular foundations. *International Journal for Numerical and Analytical Methods in Geomechanics 13*, 645–664.

Andersen, L. (2002). *Wave propagation in inifinite structures and media*. PhD thesis, Aalborg University, Denmark.

Andersen, L. and C. Jones (2001a). BEASTS — A Computer Program for Boundary Element Analysis of Soil and Three-dimensional Structures. ISVR Technical Memorandum 868, Institute of Sound and Vibration Research, University of Southampton.

Andersen, L. and C. Jones (2001b). Three-Dimensional Elastodynamic Analysis Using Multiple Boundary Element Domains. ISVR Technical Memorandum 867, Institute of Sound and Vibration Research, University of Southampton.

Andersen, L. and C. J. C. Jones (2002). Finite element addendum for BEASTS. ISVR Technical Memorandum 881, Institute of Sound and Vibration Research, University of Southampton.

Beskos, D. E. (1987). Boundary element methods in dynamic analysis. *Appl. Mech. Rev. 40*, 1–23.

Beskos, D. E. (1997). Boundary element methods in dynamic analysis: Part ii (1986-1996). *Appl. Mech. Rev. 50*, 149–197.

Das, B. M. (1993). *Principles of Soil Dynamics*. Pacific Grove, CA, USA: Brooks/Cole.

Dobry, R. and G. Gazetas (1986). Dynamic response of arbitrarily shaped foundations. *J. Engng. Mech. Div., ASCE 112*(2), 109–135.

Doherty, J. P. and A. J. Deeks (2003). Elastic response of circular footings embedded in a non-homogeneous half-space. *Géotechnique 53*(8), 703–714.

Doherty, J. P., G. T. Houlsby, and A. J. Deeks (2005). Stiffness of flexible caisson foundations embedded in non-homogeneous elastic soil. *Journal of Geotechnical and Geoenvironmental Engineering, ASCE 131*(12), 1498–1508.

Domínguez, J. (1993). *Boundary elements in dynamics*. Southampton: Computational Mechanics Publications.

Domínguez, J. (2003). *Boundary Element Methods for Soil-Structure Intercation* (1 ed.)., Chapter 1: Twenty five years of boundary elements for dynamic soil–structure interaction, pp. 1–60. Dordrecht, The Netherlands: Kluwer Academic Publishers.

Gazetas, G. and R. Dobry (1984). Simple radiation damping model for piles and footings. *J. Engng. Mech. Div., ASCE 110*(6), 931–956.

Higdon, R. L. (1990). Radiation boundary conditions for elastic wave propagation. *SIAM Journal of Numerical Analysis 27*(4), 831–870.

Higdon, R. L. (1992). Absorbing boundary conditions for acoustic and elastic waves in stratified media. *Journal of Computational Physics 101*, 386–418.

Houlsby, G. T., L. B. Ibsen, and B. W. Byrne (2005). Suction caissons for wind turbines. In *Proceedings of International Symposium on Frontiers in Offshore Geotechnics: ISFOG 2005*, Perth, Australia. Taylor & Francis Group, London.

Ibsen, L. B. and M. Liingaard (2006a). Dynamic stiffness of suction caissons—torsion, sliding and rocking. DCE Technical report 8, Department of Civil Enigineering, Aalborg University.

Ibsen, L. B. and M. Liingaard (2006b). Lumped-parameter models. DCE Technical report 11, Department of Civil Enigineering, Aalborg University.

Ibsen, L. B., M. Liingaard, and S. A. Nielsen (2005, 26 - 28 October). Bucket foundation, a status. In *Proceedings of Copenhagen Offshore Wind 2005*.

Kitahara, M. (1984). Applications of boundary integral equation methods to eigenvalue problems of elastodynamic and thin plates. Research report, University of Kyoto.

Krenk, S. (2002). Unified formulation of radiation conditions for the wave equation. *International Journal for Numerical Methods in Engineering 53*(2), 275–295.

Krenk, S. and H. Schmidt (1981). Vibration of an elastic circular plate on an elastic half-space—a direct approach. *Journal of Applied Mechanics 48*, 161–168.

Luco, J. E. and R. A. Westmann (1971). Dynamic response of circular footings. *J. Engng. Mech. Div., ASCE 97*(EM5), 1381–1395.

Pyl, L., D. Clouteau, and G. Degrande (2004). A weakly singular boundary integral equation in elastodynamics for heterogeneous domains mitigating fictious eigenfrequencies. *Engineering Analysis with Boundary Elements 28*, 1493–1513.

Richart, F. E., J. R. Hall, and R. D. Woods (1970). *Vibration of Soils and Foundations*. Englewood Cliffs, NJ: Prentice-Hall.

Senders, M. (2005). Tripods with suction caissons as foundations for offshore wind turbines on sand. In *Proceedings of International Symposium on Frontiers in Offshore Geotechnics: ISFOG 2005*, Perth, Australia. Taylor & Francis Group, London.

Veletsos, A. and Y. Tang (1987). Vertical vibration of ring foundations. *Earthquake Engineering and Structural Dynamics 15*, 1–21.

Veletsos, A. and Y. Wei (1971). Lateral and rocking vibration of footings. *J. Soil Mech. Found. Engrg. Div., ASCE 97*, 1227–1248.

Wolf, J. P. (1994). *Foundation Vibration Analysis Using Simple Physical Models*. Englewood Cliffs, NJ: Prentice-Hall.

Wolf, J. P. and C. Song (1996). *Finite-Element Modeling of Unbounded Media* (1 ed.). Chichester: John Wiley & Sons Ltd.

Appendix

Appendix A
Solution for an infinite cylinder

Consider an elastic full-space with material density ρ and shear modulus G. As depicted on Figure A.1 the full-space is divided into two domains by an infinitely long circular cylinder, the centre axis of which coincides with the x_3-axis. The interior domain is coined Ω_1, and the remaining part of the full-space, i.e. the exterior domain, is coined Ω_2. The boundary of Ω_1 is denoted Γ_1 and has the outward unit normal $\hat{\mathbf{n}}_1(\mathbf{x})$, whereas the boundary of Ω_2 is denoted Γ_2 and has the outward unit normal $\hat{\mathbf{n}}_2(\mathbf{x})$. Evidently, Γ_1 coalesces with Γ_2, and $\hat{\mathbf{n}}_1(\mathbf{x}) = -\hat{\mathbf{n}}_2(\mathbf{x})$ along the cylindrical interface, cf. Figure A.1.

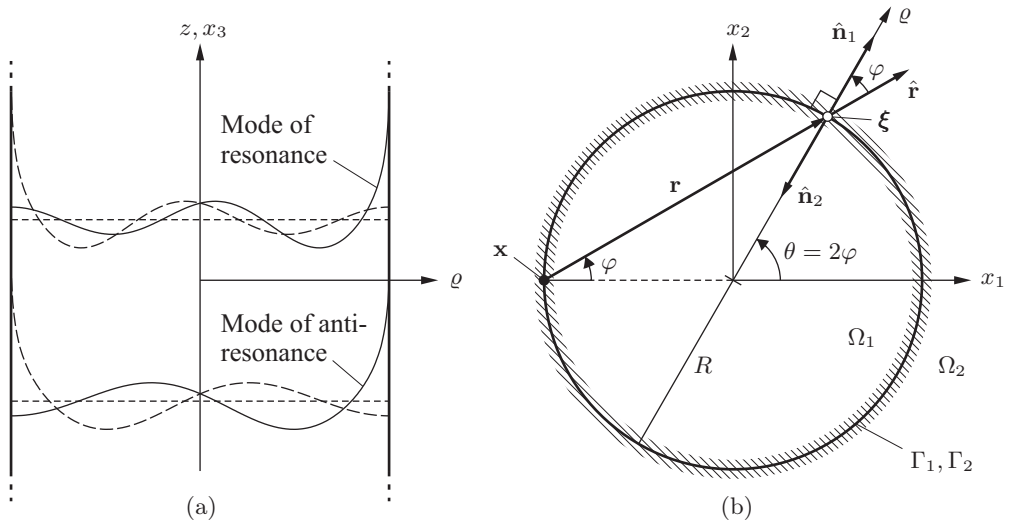

Figure A.1: Geometry of infinite cylinder and definition of polar coordinates: (a) (ϱ, z)-plane and (b) (ϱ, θ)-plane. An observation point $\mathbf{x}$ with the plane coordinates $(x_1, x_2) = (-1, 0)$ is considered, and material is present on both sides of the cylindrical interface.

The cylindrical interface between Ω_1 and Ω_2 is subject to a harmonically varying forced displacement with the cyclic frequency ω and applied in the x_3-direction, i.e. along the centre axis. This leads to pure antiplane shear wave propagation (SH-waves) in the elastic material, i.e. there is no displacement in the x_1- or x_2-direction. Depending on ω, the geometry of the cylinder and the wave propagation velocity $c_S = \sqrt{G/\rho}$, the

excitation may lead to resonance or antiresonance as illustrated on Figure A.1. Further, since the surface is smooth along the entire interface, the boundary integral equations (1.7) for the two domains are reduced to

$$\frac{1}{2}V_1(\mathbf{x},\omega)+\int_{\Gamma_1}P^*(\mathbf{x},\omega;\boldsymbol{\xi})V_1(\boldsymbol{\xi},\omega)\mathrm{d}\Gamma_{\boldsymbol{\xi}}=\int_{\Gamma_1}V^*(\mathbf{x},\omega;\boldsymbol{\xi})P_1(\boldsymbol{\xi},\omega)\mathrm{d}\Gamma_{\boldsymbol{\xi}}, \tag{A.1a}$$

$$\frac{1}{2}V_2(\mathbf{x},\omega)+\int_{\Gamma_2}P^*(\mathbf{x},\omega;\boldsymbol{\xi})V_2(\boldsymbol{\xi},\omega)\mathrm{d}\Gamma_{\boldsymbol{\xi}}=\int_{\Gamma_2}V^*(\mathbf{x},\omega;\boldsymbol{\xi})P_2(\boldsymbol{\xi},\omega)\mathrm{d}\Gamma_{\boldsymbol{\xi}}, \tag{A.1b}$$

where $V_1(\mathbf{x},\omega)$ and $V_2(\mathbf{x},\omega)$ are the displacements in the x_3-direction along the boundaries Γ_1 and Γ_2, respectively, whereas $P_1(\mathbf{x},\omega)$ and $P_2(\mathbf{x},\omega)$ are the corresponding surface tractions. Further, $P^*(\mathbf{x},\omega;\boldsymbol{\xi})$ is the surface traction related to the Green's function $V^*(\mathbf{x},\omega;\boldsymbol{\xi})$. In the case of antiplane shear waves, the fundamental solutions providing the response at the observation point $\mathbf{x}$ to a harmonically varying point force at the source point $\boldsymbol{\xi}$ are given as Domínguez (1993)

$$V^*(\mathbf{x},\omega;\boldsymbol{\xi})=\frac{1}{2\pi G}K_0(\mathrm{i}k_S r),\quad P^*(\mathbf{x},\omega;\boldsymbol{\xi})=-\frac{k_S}{2\pi}\frac{\partial r}{\partial n}K_1(\mathrm{i}k_S r),\quad r=||\mathbf{r}||_2,\quad \mathbf{r}=\mathbf{x}-\boldsymbol{\xi}, \tag{A.2}$$

where K_m is the modified Bessel function of the second kind and order m, whereas $\partial r/\partial n$ defines the partial derivative of the distance r between the source and observation point in the direction of the outward normal. With the definitions given on Figure A.1, and further introducing $\hat{\mathbf{n}}(\boldsymbol{\xi})=\hat{\mathbf{n}}_1(\boldsymbol{\xi})=-\hat{\mathbf{n}}_2(\boldsymbol{\xi})$, it becomes evident that

$$\frac{\partial r}{\partial n}=\begin{cases}\hat{\mathbf{r}}(\mathbf{x},\boldsymbol{\xi})\cdot\hat{\mathbf{n}}(\boldsymbol{\xi})=\ \cos(\varphi) & \text{for}\ \ \mathbf{x}\in\Gamma_1\\ -\hat{\mathbf{r}}(\mathbf{x},\boldsymbol{\xi})\cdot\hat{\mathbf{n}}(\boldsymbol{\xi})=-\cos(\varphi) & \text{for}\ \ \mathbf{x}\in\Gamma_2\end{cases}\qquad \text{where}\qquad \hat{\mathbf{r}}(\mathbf{x},\boldsymbol{\xi})=\frac{\mathbf{x}-\boldsymbol{\xi}}{||\mathbf{x}-\boldsymbol{\xi}||_2}. \tag{A.3}$$

Here φ is the angle between the distance vector $\mathbf{r}$ and the normal vector $\hat{\mathbf{n}}$. Finally, in Equation (A.1) k_S is the wavenumber of S-waves. In the case of hysteretic material damping with the loss factor η,

$$k_S=\frac{\omega}{c_S},\quad c_S^2=(1+\mathrm{i}\eta)\frac{G}{\rho}. \tag{A.4}$$

Now, the forced displacement is applied with constant amplitude $\hat{V}(\omega)$ and in phase along the cylindrical interface, $\Gamma\equiv\Gamma_1$. Accordingly, the traction on either side of the interface will be uniform and in phase. Continuity of the displacements across the interface then provides the result:

$$V_1(\mathbf{x},\omega)=V_2(\mathbf{x},\omega)=\hat{V}(\omega),\quad P_1(\mathbf{x},\omega)=\hat{P}_1(\omega),\quad P_2(\mathbf{x},\omega)=\hat{P}_2(\omega),\quad \mathbf{x}\in\Gamma. \tag{A.5}$$

Hence, Equation (A.1) may be rewritten as

$$\hat{V}(\omega)\left(\frac{1}{2}+\int_{\Gamma}P^*(\mathbf{x},\omega;\boldsymbol{\xi})\mathrm{d}\Gamma_{\boldsymbol{\xi}}\right)=\hat{P}_1(\omega)\int_{\Gamma}V^*(\mathbf{x},\omega;\boldsymbol{\xi})\mathrm{d}\Gamma_{\boldsymbol{\xi}}, \tag{A.6a}$$

$$\hat{V}(\omega)\left(\frac{1}{2}-\int_{\Gamma}P^*(\mathbf{x},\omega;\boldsymbol{\xi})\mathrm{d}\Gamma_{\boldsymbol{\xi}}\right)=\hat{P}_2(\omega)\int_{\Gamma}V^*(\mathbf{x},\omega;\boldsymbol{\xi})\mathrm{d}\Gamma_{\boldsymbol{\xi}}, \tag{A.6b}$$

where use has been made of Equation (A.3). Addition of Equations (A.6a) and (A.6b) provides a measure of the dynamic stiffness per unit surface of the interface related to displacement along the cylinder axis. The stiffness per unit length of the infinite cylinder then becomes

$$S_{VV}(\omega) = -L_\Gamma \frac{\hat{P}(\omega)}{\hat{V}(\omega)} = -\frac{L_\Gamma}{2\alpha}, \quad \hat{P}(\omega) = \frac{1}{2}\left(\hat{P}_1(\omega) + \hat{P}_2(\omega)\right), \tag{A.7}$$

where L_Γ is the length of the interface Γ, measured in the (x_1, x_2)-plane, and

$$\alpha = \int_\Gamma V^*(\mathbf{x}, \omega; \boldsymbol{\xi}) \mathrm{d}\Gamma_{\boldsymbol{\xi}}. \tag{A.8}$$

Equations (A.7)–(A.8) hold for arbitrary geometries of the infinite cylinder. However, in what follows a restriction is made to an infinite circular cylinder with the radius R, that is with $L_\Gamma = 2\pi R$. In order to compute α, the cylindrical polar coordinates (ϱ, θ, z) are introduced such that

$$x_1 = \varrho \cos\theta, \quad x_2 = \varrho \sin\theta, \quad x_3 = z. \tag{A.9}$$

In these coordinates, the boundary Γ is defined by $\varrho = R$, $0 \leq \theta < 2\pi$, $-\infty < z < \infty$. In particular, when an observation point $\mathbf{x}$ with the plane coordinates $(x_1, x_2) = (-1, 0)$ is considered (see Figure A.1), the distance r between the source and observation point becomes

$$r = R\frac{\sin 2\varphi}{\sin\varphi} = 2R\cos\varphi. \tag{A.10}$$

Making use of the fact that $\theta = 2\varphi$, Equation (A.8) may then be evaluated as

$$\alpha = \frac{1}{2\pi G}\int_0^{2\pi} K_0(\mathrm{i}k_S r) R \mathrm{d}\theta = \frac{1}{\pi}\frac{R}{G}\int_0^{\pi} K_0(2\mathrm{i}k_S R\cos\varphi)\mathrm{d}\varphi = -\frac{R}{G} J_0(k_S R) K_0(\mathrm{i}k_S R). \tag{A.11}$$

Here J_0 is the Bessel function of the first kind and order 0. It is noted that $K_0(\mathrm{i}k_S R) \to \infty$ for $k_S \to 0$. Hence, $S_{VV}(\omega) \to 0$ for $\omega \to 0$. Furthermore, $J_0(k_S R)$ has a number of zeros for $\eta = 0$ and $k_S > 0$. At the corresponding circular frequencies, $K^*_{VV}(\omega)$ becomes singular as reported by Kitahara (1984).